

# PCCP

Accepted Manuscript



This is an *Accepted Manuscript*, which has been through the Royal Society of Chemistry peer review process and has been accepted for publication.

*Accepted Manuscripts* are published online shortly after acceptance, before technical editing, formatting and proof reading. Using this free service, authors can make their results available to the community, in citable form, before we publish the edited article. We will replace this *Accepted Manuscript* with the edited and formatted *Advance Article* as soon as it is available.

You can find more information about *Accepted Manuscripts* in the [Information for Authors](#).

Please note that technical editing may introduce minor changes to the text and/or graphics, which may alter content. The journal's standard [Terms & Conditions](#) and the [Ethical guidelines](#) still apply. In no event shall the Royal Society of Chemistry be held responsible for any errors or omissions in this *Accepted Manuscript* or any consequences arising from the use of any information it contains.

**Determination of the depth profile distribution of guest species in microporous materials using the voltammetry of immobilized particles: application to lapachol attachment to palygorskite and kaolinite**

Antonio Doménech-Carbó\*, Mariele Martini, Francisco Manuel Valle-Algarra

*Department de Química Analítica, Universitat de València, Dr. Moliner 50. 46100 Burjassot (Valencia) Spain.*

\* Corresponding author. E-mail: antonio.domenech@uv.es

**Keywords:** Voltammetry of immobilized particles; In-depth distribution; Microporous materials; Maya blue.

**Abstract**

A model for determining the in-depth profile distribution of electroactive species hosted in inorganic microporous matrixes using the voltammetry of immobilized particles is described. The method, based on the analysis of cyclic voltammetric data at different potential scan rates, allows to determine the in-depth profile variation of the concentration of electroactive guest species as well as the evaluation of the (oxidized form)/(reduced form) concentration ratio in cases where two oxidation states of the electroactive species coexists. The application to Maya blue-type materials prepared from lapachol, a naphthoquinonic dye, and palygorskite and kaolinite clays is reported. The determination of the in-depth distribution of guest molecules is uneasy due to the heterogeneity of the clay particle size distribution and the appearance of cyclization and redox tuning reactions. Electrochemical data revealed differences in the in-depth distribution of the dye molecules in the grains of the channelled (palygorskite) and the laminar (kaolinite) clays that suggest that lapachol compounds can ingress into the channels of the palygorskite framework whereas remain externally adsorbed onto the kaolinite crystals.

## 1. Introduction

The ability of microporous inorganic materials to stabilize reactive ionic species proved to be useful in the development of electrocatalytic systems<sup>1</sup> and in the design of analytical sensors<sup>2</sup>. In most cases, bulky organic species become permanently entrapped into the voids (pores, cages, channels) of the inorganic support via the so-called ship-in-a-bottle synthetic procedures thus defining encapsulated systems. Confinement and site isolation are determinant of the peculiar reactivity of such hybrid materials.<sup>3-5</sup>

A general problem for elucidating the chemical and photochemical reactivity of the resulting materials is the determination of the distribution of the organic guests in the voids of the inorganic host<sup>6</sup>. This distribution is critical for the appearance of cooperative processes, as recently emphasized by Calzaferri.<sup>7</sup> On the other hand, the distribution of pharmacologically active guests into nanostructured materials is relevant for determining the kinetics and performance of drug delivery processes.<sup>8-10</sup>

As recently studied<sup>11-13</sup> and reviewed<sup>14</sup> by Hashimoto, methods reported for this purpose include diffuse reflectance transient absorption spectroscopy,<sup>14</sup> photoinduced electron transfer and charge separation,<sup>15-22</sup> confocal optical microscopy,<sup>23</sup> microscope FTIR mapping,<sup>24</sup> and multidimensional NMR correlation spectroscopy,<sup>25</sup> among others.<sup>14</sup> It should be noted that the influence of charge compensating ions to control the distribution and conformation of the guest species within the channels of ion-permeable microporous materials,<sup>7,14</sup> and that species distribution can influence photochemical<sup>26,27</sup> and mechanical<sup>28</sup> properties of this kind of materials.

The purpose of the current work is to report a theoretical model for determining the in-depth distribution of redox-active guest species associated to microporous inorganic supports based on the application of the voltammetry of immobilized particles (VIMP). The VIMP is a solid-state electrochemical methodology developed by Scholz et al. which provides analytical information on sparingly soluble solids upon attachment to inert electrodes in contact with suitable electrolytes<sup>29-31</sup> which has been previously applied to different organic-inorganic hybrid

materials.<sup>32-36</sup>

The presented formulation is based on the general model for the electrochemistry of ion-permeable solids provided by Lovric, Scholz, Oldham et al.<sup>37-41</sup> where the electrochemical reaction is initiated at the three-phase solid particle/base electrode/electrolyte junction further expanding through the solid particles via ion diffusion and electron hopping between immobile redox-active centers. Accordingly, the voltammetric response at different times should be representative of the advance of the diffusion layer through the immobilized particles.<sup>35,36,42</sup>

The proposed methodology is also applied to the study of the in-depth speciation of guest molecules in cases where such species can exist in two different oxidation states, using existing formulations for their electrochemical discrimination.<sup>43-46</sup> This problem is of interest in regard to the existence of redox tuning in organic guest species attached to microporous silicates,<sup>47,48</sup> in particular, to the indigo/dehydroindigo dual composition of the Maya blue.<sup>34-36</sup> Here, experimental chronoamperometric and voltammetric data are provided for a set of synthetic Maya blue-type specimens prepared from lapachol (2-hydroxy-3-(3-methyl-2-butenyl)-1,4-naphthoquinone), a naphthoquinonic dye extracted from *guachupin* plant (*Diphysa robinooides*, fam. *Fabaceae*), used as a colorant by ancient Mesoamerican people,<sup>49-51</sup> to two types of supports: i) palygorskite (PL), a fibrous phyllosilicate of ideal composition  $\text{Si}_8(\text{Mg}_2\text{Al}_2)\text{O}_{20}(\text{OH})_2(\text{H}_2\text{O})_4 \cdot 4\text{H}_2\text{O}$ , and ii) kaolinite (KA), a laminar clay of composition  $[\text{Al}_2\text{Si}_2\text{O}_5(\text{OH})_4]$ , where the dye cannot undergo encapsulation, testing specimens prepared at room temperature and specimens treated at temperatures between 100 °C and 180 °C. This thermal treatment favors dye association to the clays and redox tuning of the guest species.<sup>42,47,48</sup> Preliminary data suggesting the existence of redox tuning upon lapachol (LA) attachment to phyllosilicates were previously reported.<sup>52</sup>

It is pertinent to note that the distribution of guest species can influence notably the effectiveness of drug delivery from drug encapsulated into microporous hosts, as recently reviewed by Arruebo.<sup>53</sup> Lapachol, and several analogues and derivatives, all exhibiting exhibit antitumor, antibiotic, antimalarial, anti-inflammatory and antiulceric activities,<sup>54,55</sup> could be considered as model compounds for testing the performance of drug encapsulation/delivery.

## 2. Experimental

Dye-clay hybrid specimens were prepared by finely grinding in an agate mortar and pestle 1.00 g of the clay with 1% wt lapachol (Extrasynthèse) in an agate mortar and pestle during 60 min. The resulting specimens were separated in different aliquots of 0.10 g some of which were maintained at room temperature (25 °C) (in the following labeled as dye@clay<sub>25</sub>) and several others were submitted to heating at temperatures between 100 °C and 150 °C in furnace during 24 h (labeled as dye@clay<sub>t</sub>). Palygorskite (collected from the *Sak lu'um* classical site in Yucatan) and kaolinite (obtained from the repository of the Clay Mineral Society) were used as received. In order to ensure minimal excess of non-attached dye, the initial proportion of dye to clay (1% w/w) in such samples was taken below the theoretical maximum of ca. 4 % w/w estimated for dye@palygorskite hybrid.<sup>34,35</sup> The thermal treatment, producing the partial loss of zeolitic water of the clays, is a precondition to obtain stable pigmenting materials having a strong dye@clay association in the case of phyllosilicate hybrids.<sup>34,35</sup> Blank experiments were also performed with PL and KA clays and dye samples.

The prepared dye@clay specimens were characterized by X-ray diffraction (XRD), scanning electron microscopy (SEM), transmission electron microscopy (TEM), attenuated total reflectance-Fourier transform infrared spectroscopy (ATR-FTIR), Vis-UV diffuse reflectance spectroscopy and scanning electrochemical microscopy (SECM), as previously described<sup>52</sup> (see also Supplementary information). Testing the dye composition in such specimens was performed by means of high-performance liquid chromatography with diode array detection (LD-DAD) and ultra performance liquid chromatography/mass spectroscopy (UPLC-MS) applied to the extracts obtained from the specimens using conventional extraction procedures with MeOH, DMSO and different MeOH/water and DMSO/water mixtures as already described.<sup>52</sup>

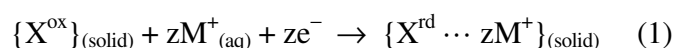
Cyclic voltammograms (CV), square wave voltammograms (SQWV) and chronoamperograms (CA) were performed with a CH 660I potentiostat in a cell thermostated at 298±1 K. VIMP experiments

were performed using sample-modified paraffin-impregnated graphite electrodes (PIGEs) consisting of graphite rods impregnated *in vacuo* with paraffin as described in literature.<sup>29,30</sup> For modified electrode preparation the clay samples were thoroughly powdered in an agate mortar and pestle and extended forming a spot of finely distributed material. The lower end of the graphite electrode was pressed over that spot of sample to obtain a sample-modified surface. Chronoamperograms (CA) were performed on films of the prepared materials on glassy carbon electrode (area 0.071 cm<sup>2</sup>) prepared by drop casting method by evaporation of a drop (50  $\mu$ L) suspensions (1 mg/mL) of the hybrid materials in ethanol. An Ag/AgCl (3M NaCl) reference electrode and a platinum-wire auxiliary electrode completed the three-electrode arrangement.

### 3. Results and discussion

#### 3.1. Modeling in-depth electrochemistry

The proposed model is based on a series of simplifying assumptions on the voltammetry of ion-insertion solids which can be summarized as: (i) the electrochemical process occurs in the porous material via coupled electron hopping between immobile redox centers and diffusion of charge-balancing ions through the porous matrix; (ii) the overall process can be considered as diffusion-controlled with no influence of migration/resistance effects; (iii) mono-dimensional, relatively slow diffusion is considered so that the size of the grains of porous material is large compared to the size of the diffusion layer so that semiinfinite boundary conditions for planar diffusion can be applied. Accordingly, let us consider the reduction of a microparticulate deposit on an inert electrode of an ion-permeable solid containing immobile redox centers. In agreement to the model of Lovric, Scholz, Oldham and co-workers,<sup>37-41</sup> the electrochemical process is initiated at the particle/base electrode/electrolyte three-phase junction and progress via ion diffusion through the solid and electron hopping between the redox centers. This process can be represented as:



where { } denote solid materials. As a particular case, electrolyte charge-balancing cations can be

hydrogenions. For a microparticulate deposit of such ion-insertion solids, the current will depend on the shape and size of the particles, the concentration of immobile redox centers in the solid and the diffusion coefficients for electrons and cations through the solid. There are several possible situations where the current formulation is potentially applicable: (i) redox active molecules diffusing out of the pores, (ii) charge balancing ions diffusing into the pores with fast electron hopping, (iii) charge balancing ions diffusing out of the pores with fast electron hopping, (iv) slow electron hopping between immobile redox active molecules with fast diffusion of charge-balancing ions. In the most general formulation, the above cases could be described in terms of different diffusion coefficients, corresponding to the process of electron hopping between immobile redox centers ( $D_e$ ), ion transfer through the pores ( $D_{M,int}$ ) and out of the pores ( $D_{M,out}$ ), and the diffusion of redox active molecules out of the pores ( $D_{X,out}$ ). The model would be applicable to the situations (ii) and (iv) providing that two simplifying assumptions conditions are accomplished: a) the geometry of the diffusion problem can be treated as monodimensional; b) there is a unique rate-determining process so that the overall reaction rate can be expressed in terms of the corresponding diffusion coefficient or, alternatively, there is possibility of representing the overall diffusion problem in terms of an averaged diffusion coefficient  $D$ .<sup>56</sup> The cases (i) and (iii) where 'external' diffusion is involved should in principle be excluded because it is uncertain to what extent the diffusion of the redox active species out of the pores could be representative of the in-depth distribution of such species into the porous material. As already reported,<sup>57,58</sup> in cases where ion transport (or electron transport) are rate determining, such systems can be described in terms of an average diffusion coefficient usual semi-infinite boundary conditions to describe the diffusion problem. In these circumstances, the diffusion coefficient of charge carriers through the solid material can be estimated from chronoamperometric data using the mean concentration of electroactive centers in the solid, with values falling in the  $10^{-9} - 10^{-11}$  cm<sup>2</sup>/s range.<sup>36</sup>

In order to study the in-depth electrochemical response of this type of systems, we adopt the description of Oh and Nair<sup>59</sup> for the transport of organic molecules in a polycrystalline porous membrane. Let us consider a physical property,  $\xi$ , whose intensity is proportional to the concentration of guest molecules,  $c$ . When the guest molecules are heterogeneously distributed at steady state in the film, the signal intensity for a particular sampling depth,  $x$ , can be expressed as:

$$\xi(x) = \int_{x=0}^x g c(x) dx \quad (2)$$

Here,  $g$  denotes the specific response of the quantity  $\xi$  per unit concentration of the guest species for a guest-templated microporous film. The membrane with a continuously varying distribution of guest species is discretized into  $N$  sublayers, each one of thickness  $\delta_j$ , within which the guest concentration,  $c_j(x)$ , is uniform, as schematized in Figure 1. This is a laterally averaged concentration over the sublayer, thus averaging out possible inhomogeneities in the concentration between different grains in the polycrystalline film. If the sampling depth extends to  $n$  sublayers, Eq. (2) can be rewritten as:

$$\xi_n(x) = \sum_{j=1}^n g c_j(x) \delta_j \quad (3)$$

where  $c_j(x)$  represents the (average) concentration of the guest species in the  $j^{\text{th}}$  sublayer. In the following, it will be assumed that the electrochemical coefficient of response  $g$  is a concentration-independent quantity.

We assume that the electrochemical process is controlled by diffusion of electrolyte cations and electrons through the microporous crystal so that, during the time duration of the voltammetric experiment,  $t$ , the diffusion layer advances from the external surface of the microporous film deposited on the electrode ( $x=0$ , see Fig. 1) to a depth  $x$ , corresponding to the  $n^{\text{th}}$  layer in which the film is arbitrarily divided. For CVs of microporous-associated species in contact with concentrated electrolytes able to permeate the microporous, the peak potential,  $i_p$ , recorded at a given potential scan rate,  $\nu$ , can be expressed as:

$$i_p = g c_n(x) \nu^{1/2} \quad (4)$$

Where  $c_n(x)$  denotes the average concentration of immobile redox centers in the solid film between  $x = 0$  and  $x_n$ .

Notice that if the (effective) diffusion coefficient,  $D$ , is known, the depth of the  $n^{\text{th}}$  layer can be estimated as the distance advanced by the diffusion layer at the time  $t$  of experimentation:<sup>7</sup>

$$x_n = (2Dt)^{1/2} \quad (5)$$

In CV experiments, this characteristic time can be estimated as:

$$t = \frac{\Delta E_\lambda}{\nu} \quad (6)$$

$\Delta E_\lambda$  being the difference between the extreme (switching) potentials in the CV.

It is pertinent to note that the above considerations are based on the assumption that a purely diffusive behavior operates. This implies that migration/resistance effects conceivably operating to some extent in porous systems are negligible. For this purpose, integration of current/potential curves in the voltammetric peaks was performed and the (charge passed)/ $\nu^{1/2}$  ratio was determined. As far as constant values were obtained for such ratio for the different studied voltammetric signals, diffusion-controlled conditions were taken as operative under our experimental conditions. As previously noted, it will be assumed that the diffusion is slow enough to consider non-critical the size of the grains of the porous material and formulate the diffusion problem in terms of monodimensional diffusion.

As far as peak potentials in voltammetric experiments on ion-insertion solids became essentially independent on the concentration of redox centers,<sup>38</sup> the variation of the (peak current)/ $\nu^{1/2}$  ratio with  $\nu$  was taken as representative of the in-depth variations of the concentration of the immobile redox centers. Then, if the immobile electroactive centers of the solid are uniformly distributed within the film,  $c_n(x) = \text{constant}$  regardless  $n$ . the  $i_p$  vs.  $\nu^{1/2}$  plot should be linear and, accordingly, the

variation of  $I = i_p/v^{1/2}$  on  $v$  should be a horizontal straight line. In the studied systems (*vide infra*), however, we obtain variations such as depicted in Figure 2, where  $I (= i_p/v^{1/2})$  vs.  $v$  plots for graphite electrodes modified with LA@PL<sub>150</sub> and LA@PL<sub>25</sub> immersed into 0.25 M aqueous acetate buffer at pH 4.75 are shown. Apparently,  $I$  reaches a certain limiting value at  $v = 0$ ,  $I_o$ , and tends to a limiting value at high potential scan rates,  $I_{lim}$ .  $I_o$ , formally corresponding to an infinite time measurement, could be taken as representative of the average composition of the overall electroactive region of the solid grains, given by an average concentration  $c_{av}$ , of the guest molecules. In turn,  $I_{lim}$  could be taken as representative of the concentration of guest species in the more external layer of the material. Accordingly, we can take:

$$I_n(x) = gc_n(x) \quad (7)$$

$$I_o = gc_{av} \quad (8)$$

$$I_{lim} = gc_{boundary} \quad (9)$$

Here,  $c_n(x)$  denotes the average concentration of electroactive centers in the solid in the region between  $x = 0$  and the  $n^{\text{th}}$  layer and  $c_{boundary}$  the concentration of such centers in the boundary of the film; i.e., at  $x = 0$ .

If the solid film is modeled by a series of layers, as previously described, one can write:

$$I_n(x) = \frac{\sum_{j=1}^n gc_j(x)\delta_j}{\sum_{j=1}^n \delta_j} = \frac{\sum_{j=1}^n gc_j(x)\delta_j}{x_n} \quad (10)$$

$$I_{n+1}(x) = \frac{\sum_{j=1}^{n+1} gc_j(x)\delta_j}{\sum_{j=1}^{n+1} \delta_j} = \frac{\sum_{j=1}^{n+1} gc_j(x)\delta_j}{x_{n+1}} \quad (11)$$

The difference in the  $I$  values relative to the boundary concentration between two consecutive

layers can be expressed as:

$$\frac{I_{n+1}(x)}{I_{\text{lim}}} - \frac{I_n(x)}{I_{\text{lim}}} = \frac{\sum_{j=1}^{n+1} g c_j(x) \delta_j}{g c_{\text{boundary}} x_{n+1}} - \frac{\sum_{j=1}^n g c_j(x) \delta_j}{g c_{\text{boundary}} x_n} \quad (12)$$

Introducing the thickness of the  $k$ -layer,  $\delta_k (= x_{n+1} - x_n)$  and the concentration of this layer,  $c_k$ , one can write:

$$\sum_{j=1}^{n+1} g c_j(x) \delta_j = \sum_{j=1}^n g c_j(x) \delta_j + g c_k \delta_k \quad (13)$$

we can obtain:

$$\frac{I_{n+1}(x)}{I_{\text{lim}}} - \frac{I_n(x)}{I_{\text{lim}}} = \frac{x_n \delta_k c_k - \delta_j \sum_{j=1}^n c_j(x) \delta_j}{c_{\text{boundary}} x_n x_{n+1}} \quad (14)$$

$$\frac{I_{n+1}(x)}{I_{\text{lim}}} - \frac{I_n(x)}{I_{\text{lim}}} = \frac{x_n \delta_k c_k}{c_{\text{boundary}} x_n x_{n+1}} - \frac{\delta_k I_n(x)}{c_{\text{boundary}} x_{n+1}} \quad (15)$$

As a result, we can estimate the average concentration of the  $k$ -layer relative to the boundary concentration as:

$$\frac{c_k}{c_{\text{boundary}}} = \left( \frac{I_{n+1}(x)}{I_{\text{lim}}} - \frac{I_n(x)}{I_{\text{lim}}} \right) \left( \frac{x_{n+1}}{\delta_k} \right) + \frac{I_n(x)}{I_{\text{lim}}} \quad (16)$$

Let us consider the case of immobile redox centers coexisting in two interconnected species (eventually the oxidized and reduced forms of a given guest) A and B, so that the molar fraction of the form A,  $\alpha_A$ , varies with depth. In the most favorable case, the species A and B produce separate,

diffusion-controlled voltammetric signals whose experimental peak currents ( $i_p^A$ ,  $i_p^B$ ) permit to determine the corresponding  $i_p/v^{1/2}$  ratios,  $I^A$ ,  $I^B$ . Then, the following relationships should be satisfied:

$$I_n^A(x) = \frac{\sum_{j=1}^n g^A c_j^A(x) \delta_j}{\sum_{j=1}^n \delta_j} = \frac{\sum_{j=1}^n g^A c_j^A(x) \delta_j}{x_n} \quad (17)$$

$$I_{n+1}^B(x) = \frac{\sum_{j=1}^{n+1} g^B c_j^B(x) \delta_j}{\sum_{j=1}^{n+1} \delta_j} = \frac{\sum_{j=1}^{n+1} g^B c_j^B(x) \delta_j}{x_{n+1}} \quad (18)$$

as well as expressions equivalent to Eqs. (7)-(9). We can write:

$$I_{n+1}^A(x) - I_n^A(x) = \frac{\sum_{j=1}^{n+1} g^A c_j^A(x) \delta_j}{\sum_{j=1}^{n+1} \delta_j} - \frac{\sum_{j=1}^n g^A c_j^A(x) \delta_j}{\sum_{j=1}^n \delta_j} \quad (19)$$

$$I_{n+1}^B(x) - I_n^B(x) = \frac{\sum_{j=1}^{n+1} g^B c_j^{\text{tot}}(x) \delta_j}{\sum_{j=1}^{n+1} \delta_j} - \frac{\sum_{j=1}^n g^B c_j^{\text{tot}}(x) \delta_j}{\sum_{j=1}^n \delta_j} \quad (20)$$

Using the precedent formalism to the A- and B-localized signals, the average molar ratio between the forms A and B at the  $k$ -layer located between the  $n^{\text{th}}$  and  $(n+1)^{\text{th}}$  layers,  $f_k^A$ , can be calculated as:

$$f_k^A = \frac{(c_A/c_B)_k}{(c_A/c_B)_{\text{boundary}}} = \frac{\left(\frac{x_{n+1}}{\delta_k}\right) \left[ \frac{I_{n+1}^A(x)}{I_{\text{lim}}^A} - \frac{I_n^A(x)}{I_{\text{lim}}^A} \right] - \left( \frac{I_n^A(x)}{I_{\text{lim}}^A} \right)}{\left(\frac{x_{n+1}}{\delta_k}\right) \left[ \frac{I_{n+1}^B(x)}{I_{\text{lim}}^B} - \frac{I_n^B(x)}{I_{\text{lim}}^B} \right] - \left( \frac{I_n^B(x)}{I_{\text{lim}}^B} \right)} \quad (21)$$

Another possibility is the disposal of independent, diffusion-controlled signals for one of the components and the total guest (as occurring for the lapachol@clay systems, *vide infra*). Then, if the signal representative of the total guest displays a  $i_p/v^{1/2}$  ratio  $I$ , one can relate the molar fraction of the A component at the  $k$ -layer,  $\alpha_k^A$ , defined as:

$$\alpha_k^A = \left( \frac{c_A}{c} \right)_k \quad (22)$$

to the corresponding molar fraction at the boundary region,  $\alpha_{\text{boundary}}^A = (c_A/c)_{\text{boundary}}$ , by means of the relationship:

$$\frac{\alpha_k^A}{\alpha_{\text{boundary}}^A} = \frac{\left(\frac{x_{n+1}}{\delta_k}\right) \left[ \frac{I_{n+1}^A(x)}{I_{\text{lim}}^A} - \frac{I_n^A(x)}{I_{\text{lim}}^A} \right] - \left( \frac{I_n^A(x)}{I_{\text{lim}}^A} \right)}{\left(\frac{x_{n+1}}{\delta_k}\right) \left[ \frac{I_{n+1}^B(x)}{I_{\text{lim}}^B} - \frac{I_n^B(x)}{I_{\text{lim}}^B} \right] - \left( \frac{I_n^B(x)}{I_{\text{lim}}^B} \right)} \quad (23)$$

Using this equation, it is possible to calculate the molar fraction of oxidized form at the  $k$ -layer from CV data.

### 3.2. Characterization of the materials

The prepared dye@clay specimens were characterized by XRD, transmission electron microscopy (TEM), ATR-FTIR and Vis-UV diffuse reflectance spectroscopy as previously described.<sup>52</sup> In agreement with data for other Maya Blue-type hybrids having low dye loadings, the diffractogram and infrared spectra (see Supplementary materials, Fig. S.1) were essentially identical to those of

the pristine clays.<sup>47,48</sup> TEM examination of the prepared specimens revealed the presence of aggregates of acicular crystals 0.5-1  $\mu\text{m}$  sized having fine fiber structures with thickness from 300 to 600  $\text{\AA}$  in the deposits of palygorskite and LA@PL<sub>25</sub>. In thermally treated, specimens, significant textural changes were observed, consisting of the appearance of a more or less dense array of pores in the crystal surface (see Figure 3 and Supplementary materials, Fig. S.2). This feature can be attributed to the evacuation of zeolitic water during the applied thermal treatment at temperatures above 100  $^{\circ}\text{C}$ .<sup>47,48</sup> Kaolinite deposits consisted of pseudo-hexagonal crystals 0.2-0.5  $\mu\text{m}$  sized. The specific surface area was of 60 and 25  $\text{g}/\text{m}^2$  for palygorskite and kaolinite, respectively whereas the micropore specific volumes were of 0.050 and 0.025  $\text{cm}^3/\text{g}$ , respectively. Such values were in agreement with those in literature for palygorskite<sup>60,61</sup> and kaolinite.<sup>62</sup> The channels of palygorskite are  $3.7 \times 6.4$   $\text{\AA}$  sized.<sup>61</sup>

LC-DAD and UPLC-MS experiments on aliquots of the extracts obtained upon rinsing the pristine clays with different solvents (MeOH, DMSO) do not show presence of organic impurities. Performing the same extraction experiments in dye@clay<sub>25</sub> materials denoted, as already described,<sup>52</sup> that in the external regions lapachol was the unique organic component. However, in the extractable portion of thermally treated dye@clay specimens (i.e., the 'externally' adsorbed dye molecules), the parent lapachol was accompanied by several other isomer compounds, namely,  $\alpha$ -lapachone, and other lapachones, 4-hydroxy- $\alpha$ -lapachone, dihydro-4-hydroxy- $\alpha$ -lapachone and a unique oxidized compound, dehydro- $\alpha$ -lapachone (see Table S.1 and Fig. S.3 in Supplementary information). As far as the voltammetric response (*vide infra*) revealed that the reduction of the parent lapachol and their isomers occurs at a similar potential, the system will be treated as constituted by a unique reduced form and a unique oxidized one, as discussed below.

The electrodes prepared by means of the drop-casting method showed an irregular distribution of crystals and aggregates of crystals in contact with the base electrode, as depicted in Figure 3. The TEM and SECM images suggest that, upon gravity-driven deposition the crystals contact well with the base electrode. Under these conditions, and assuming that slow diffusion of charge carriers through the crystals occur, the system could be approached to a film with 1D diffusion. This situation is in principle close to that reported in literature for metal-oxide modified electrodes<sup>63</sup> and

different aluminosilicate materials.<sup>44-48</sup>

### 3.3. Electrochemistry of LA@PL and LA@KA materials

Figure 4 shows CV of microparticulate deposits of: a,b) lapachol, c,d) LA@KA<sub>25</sub>, in contact with aqueous acetate buffer at pH 4.75. Upon scanning the potential in the negative direction, lapachol crystals display a cathodic peak at  $-0.48$  V vs. Ag/AgCl ( $C_1$ ) whose anodic counterpart ( $A_1$ ) is absent. In the subsequent anodic scan, oxidation peaks at  $+0.06$  V ( $A_2$ ) and  $+0.97$  V ( $A_3$ ) appear. In the initial anodic scan voltammograms, the peak  $A_3$  becomes well-defined and is followed, in the subsequent cathodic scan, by the peak  $C_1$ . The initial cathodic scan voltammogram of LA@KA<sub>25</sub> was similar; however, in the initial anodic scan voltammogram, two overlapping reduction signals at  $-0.24$  ( $C_2$ ) and  $-0.48$  V ( $C_1$ ) appear in the cathodic scan subsequent to peak  $A_3$ . Such peak are coupled to anodic signals at  $-0.20$  ( $A_1$ ) and  $+0.06$  V ( $A_2$ ) while the peak  $A_3$  is clearly diminished. Such differences are reinforced in palygorskite specimens, whose voltammograms are depicted in Figure 5. In the case of LA@PL<sub>25</sub>, the peak  $A_3$  becomes considerably diminished whereas the  $C_2/A_2$  couple is increased at the expense of the  $C_1/A_1$  one. In the voltammograms of LA@PL<sub>150</sub>, the peak  $A_3$  is almost entirely absent while the couple largely predominates and is preceded by an additional couple ( $C_4/A_4$ ) at  $-0.10$  V.

These features can be rationalized in the light of studies on the reductive electrochemistry of lapachol in nonaqueous<sup>64</sup> and aqueous<sup>65</sup> media and attached to carbon paste electrode with electrolyte binder in contact with aqueous electrolytes,<sup>66</sup> the oxidative electrochemistry of isolapachol<sup>67</sup> and the voltammetry of lapachones,<sup>68,69</sup> on attributing the  $C_1/A_1$  couple to the proton-assisted reduction of the quinone motif. The above redox process would be accompanied by keto-enol rearrangement, yielding a different triol species whose oxidation ( $A_2$ ) yields a quinone different to the parent compound. In turn, the peak  $A_3$  can be attributed to the oxidation of the parent lapachol to dehydrolapachone whose subsequent reduction gives rise to a lapachone, responsible of the  $C_4/A_4$  couple. UPLC-MS data confirmed the presence of  $\alpha$ -lapachone and other lapachone isomers, 4-hydroxy- $\alpha$ -lapachone, dehydro- $\alpha$ -lapachone and

dihydro-4-hydroxy- $\alpha$ -lapachone in LA@PL<sub>150</sub> specimens.<sup>52</sup>

The proposed electrochemical processes, which are schematized in Figure 6, become strongly conditioned by the attachment to the clays. As previously proposed,<sup>52</sup> lapachol attachment to palygorskite is accompanied by cyclicization and redox tuning reactions determining the formation of a significant amount of clay-associated dehydrolapachone determining the disappearance of peak A<sub>3</sub> and the concomitant appearance of the C<sub>4</sub>/A<sub>4</sub> couple. Interestingly, lapachol attachment to the palygorskite framework increases the reversibility of the voltammetric processes (except the oxidation step A<sub>3</sub>).

For our purposes, the relevant point to emphasize is that: i) lapachol attachment to palygorskite involves significant redox tuning and cyclicization reactions while attachment to kaolinite does not provide comparable results, in agreement with previous data;<sup>52</sup> ii) the differences in the behavior of LA@KA and LA@PL materials should be reflected in differences in the in-depth distribution of the guest molecules into the clay crystals. Such differences will be tested, as detailed in the following section, using chronoamperometric and voltammetric data.

In view of the above described electrochemical response of the LA@PL and LA@KA systems, there are two main difficulties for testing the model described in the section 3.1 using such systems: (i) the size distribution of the clay crystals can condition the in-depth concentration profile of the dye; (ii) the parent lapachol is accompanied by several other organic compounds (lapachones, dehydrolapachone) forming a multicomponent system. In regard to the first difficulty, it can be adduced that the shape and size distribution of both palygorskite and kaolinite crystals exhibits a reasonable homogeneity as derived from TEM image analysis.<sup>47,48</sup> The second difficulty can be reasonably bypassed on considering the similarity in the reduction signals for lapachol and the lapachones (peaks C<sub>1</sub>, C<sub>2</sub>), so that the peak current for the C<sub>1</sub>+C<sub>2</sub> signal (see for instance Figure 3d) can be taken as representative of the total concentration of lapachol and the lapachone derivatives. As far as chronoamperometric experiments (*vide infra*) were performed at a potential negative enough for promote the diffusion-controlled reduction of all these compounds, one can assume that the obtained current/time response is representative of the total concentration of lapachol plus

lapachones. The second set of voltammetric data, based on the measurement of the peak current of peak A<sub>3</sub>, yields current/time responses representative of the in-depth distribution of a unique oxidized compound, dehydrolapachone.

### 3.4. In-depth profile data analysis

As shown in Figure 3, nonlinear  $I (= i_p/v^{1/2})$  vs.  $v^{1/2}$  plots were obtained for lapachol@clay specimens, a feature that, as discussed in the precedent section, can be attributed to the in-depth variation of the concentration of electroactive species within the solid material. Using Eqs. (5) and (6), one can estimate the depth reached by the diffusion layer in the clay coating in CV experiments depending on the potential scan rate and the separation between the switching potentials upon inserting an appropriate value for the diffusion coefficient. For this purpose, chronoamperometric data can be used assuming that, at sufficiently short times, the system can be treated as having a uniform concentration of electroactive guests. According to the Lovric, Scholz and Oldham modeling,<sup>37-41</sup> chronoamperograms can be fitted to a Cottrell-like behavior approached by:<sup>57,58</sup>

$$i = \frac{nFA_{\text{eff}}c_{\text{eff}}D_{\text{eff}}^{1/2}}{2\pi^{1/2}t^{1/2}} \quad (24)$$

where  $A_{\text{eff}}$  represents an effective area of the microparticulate deposit and  $c_{\text{eff}}$  the effective concentration of guest in the solid.  $D_{\text{eff}}$  is representative of the diffusion of electrons and charge-balancing ions through the solid. Figure 7 shows the Cottrell plots of current vs.  $(\text{time})^{-1/2}$  using chronoamperometric data for LA@PL<sub>150</sub> in contact with acetate buffer at an applied potential of  $-0.45$  V. At this potential, the reduction of the dye should occur under diffusion-controlled conditions. In agreement with the previous consideration, the short-time region of the chronoamperogram shows a linear dependence of  $i$  on  $t^{-1/2}$ . Using the nominal concentration of dye in the clays (1% wt) and taking a value of  $2.0 \text{ g/cm}^3$  for the clay density and the geometric electrode area ( $0.071 \text{ cm}^2$ ), data such as in Figure 7 permit to estimate values for the diffusion coefficient of charge carriers across clays of ca.  $1.1 \times 10^{-11} \text{ cm}^2/\text{s}$ , in agreement with data for zeolites and other dye@clay materials.<sup>32,42,46,56</sup> Using this value for estimating  $x$ , the in-depth variation of the concentration of guest species was obtained from CV data such as in Figure 5 using Eq. (16). The

variation of  $I (= i_p/v^{1/2})$  on  $v$  for CV at LA@PL<sub>25</sub>-modified electrodes was shown in Figure 3, where data points for peaks C<sub>1</sub> and A<sub>3</sub> are shown. In both cases, 'saturation' curves were obtained in agreement with the foregoing set of considerations. From which, application of the proposed modeling yields the variation of  $c_j(x)/c_{\text{boundary}}$  using voltammetric data at different potential rates. Figure 8 shows the results for the studied hybrids using Eq. (18) taking depth intervals of ca.  $1 \times 10^{-5}$  cm calculated from Eq. (5) taking  $D_{\text{eff}} = 1.1 \times 10^{-11}$  cm<sup>2</sup>/s. One can see that the concentration of guest lapachol (plus different lapachones) in kaolinite specimens decreases rapidly with the depth, whereas a more smooth dependence of the guest concentration on the depth appears for palygorskite specimens. In agreement with reported data for Maya blue-type materials,<sup>35,42,47,48</sup> the guest penetrates more deeply into the clay crystals in the case of LA@PL<sub>150</sub> than in LA@PL<sub>25</sub>. Considering that palygorskite crystals are typically constituted by elongated crystals 0.5-2  $\mu\text{m}$  sized, the data obtained applying the electrochemical model suggest that, in the case of LA@PL<sub>150</sub>, the guest can penetrate deeply into the crystals. In this regard, it is pertinent to note that the depth values depend critically on the value of  $D$ , whose estimate involves a set of simplifying assumptions. A more realistic description, however, involves: i) more accurate consideration of the intracrystalline charge transfer problem considering the three-directional diffusion;<sup>37-41</sup> ii) the replacement of the continuous solid film, used here for modeling purposes, by a microparticulate deposit of clay crystals where the penetration of the guest molecules could occur in different crystal faces. As a result, the  $x$  values in Figure 8 are probably overestimated.

In spite of these limitations, the reported model provides a satisfactory picture of the guest distribution into the inorganic support. In particular, it is in agreement with the previous kinetic study on indigo@palygorskite hybrid materials,<sup>70</sup> suggesting that the formation process of such materials occurs in two consecutive steps, the first one consisting of the coupled loss of zeolitic water of the palygorskite coupled with clay-dye attachment and redox tuning and the second consisting of the diffusion-controlled penetration of the dye molecules in the palygorskite channel system.

The observed in-depth variation of the guest concentration would be also consistent with literature data for, among others, (2,2'-bipyridine)ruthenium complexes encapsulated in zeolite Y,<sup>71-73</sup> where, for larger ruthenium loadings, the complex tends to accumulate toward the surface of the zeolite

microcrystals instead of a random distribution in the aluminosilicate bulk.

Considering the previously described electrochemistry of lapachol@clay materials, one can assume that the peak current of the process  $A_3$  recorded in the initial anodic scan voltammograms such as in Figs. 4b,d,  $i_p(A_3^{1st})$ , is representative of the concentration of oxidizable lapachol (i.e., lapachol that was not previously oxidized to dehydrolapachone) whereas the peak current for the  $C_1$  plus  $C_2$  signal,  $i_p(C_{1+2}^{2nd})$ , is representative of the total concentration of lapachol (plus different lapachones) species; i.e., lapachol plus dehydrolapachone, existing in the original material. Accordingly, the  $i_p(A_3^{1st})/i_p(C_{1+2}^{2nd})$  ratio will be representative of the molar fraction of lapachol in the specimen. Figure 9 shows the variation of the  $i_p(A_3^{1st})/i_p(C_{1+2}^{2nd})$  ratio with the potential scan rate  $\nu$  for CVs PIGEs modified with LA@PL<sub>25</sub> and LA@PL<sub>150</sub>. One can see in this figure that significant differences appear between thermally treated and untreated specimens. In the case of LA@PL<sub>25</sub>, the peak current ratio first increases on increasing  $\nu$  until a maximum value is attained at ca. 100 mV/s, subsequently decreasing slowly. In contrast, for LA@PL<sub>150</sub>, the  $i_p(A_3^{1st})/i_p(C_{1+2}^{2nd})$  ratio increases monotonically. Such data can be interpreted on assuming that all lapachol forms remain externally adsorbed onto the crystals of the laminar clay kaolinite whereas can be distributed within the pore/channel system of the palygorakite clay, the penetration being favored by the application of thermal treatments.

The above voltammetric data permit to calculate the variation of the molar fraction of oxidized lapachol forms at the  $k$ -layer, relative to the molar fraction at the crystal boundary,  $\alpha_k^{ox} / \alpha_{boundary}^{ox}$ . Figure 10 shows the in-depth variation of this ratio in LA@PL<sub>25</sub> and LA@PL<sub>150</sub> materials determined from Eq. (23) using CV data. In agreement with previous data on dye@clay hybrid materials,<sup>34,35,42,47,48,52</sup> the samples submitted to thermal treatment produced larger yields of oxidized forms than the room temperature specimens, the proportion of such forms increasing on increasing the temperature from LA@PL<sub>100</sub> to LA@PL<sub>180</sub> specimens. In the case of LA@PL<sub>25</sub>, the proportion of oxidized forms of lapachol first increases with the depth until a certain maximum, subsequently decreasing upon increasing the dye penetration into the clay crystals. In contrast, in the case of LA@PL<sub>150</sub>, the relative amount of dehydrolapachone forms increases in stepwise manner upon

increasing the depth.

The foregoing set of data support the idea that voltammetric measurements can be used to determine the in-depth distribution of electroactive species into microporous solids. The validity of the proposed approach is conditioned, however, by the confidence level of the simplifying assumptions used in modeling the electrochemical response of such materials; in particular, it is conditioned by the ionic permeability of the porous solid and the possibility of electron diffusion via electron hopping between immobilized redox centers.

#### 4. Conclusions

A model is proposed for determining the in-depth distribution of electroactive guest species in microporous solid supports based on the voltammetry of immobilized particles methodology. The in-depth variation of the concentration of electroactive guest species and the (oxidized form)/(reduced form) concentration ratio, in cases where two oxidation states of the electroactive species coexists, can be calculated from cyclic voltammetric data at different potential scan rates. Application of the proposed methodology to hybrid materials constituted by lapachol associated to palygorskite and kaolinite showed significant differences depending on the type of clay. In the case of the laminar clay kaolinite, the lapachol concentration decreases rapidly, denoting that the dye is located exclusively in the external region of the clay crystals. In the case of the hybrid materials prepared from palygorskite, there is a relatively smooth in-depth variation of guest concentration, that distribution being notably conditioned by the thermal treatment applied to the sample during its preparation. Similarly, the in-depth variation of the lapachol/dehydrolapachone ratio estimated from voltammetric data varied similarly from room temperature specimens to materials prepared by thermal treatment.

The proposed approach involves a series of simplifying assumptions concerning ion and electron diffusion through the clay network and would be in principle restricted to measurements in the external boundary region of the solid particles. It is pertinent to note that the heterogeneity in the shape and size distribution of clay crystals and the presence of several dye guest molecules attached

to the clay host, can difficult significantly the application of the proposed formulation to estimate the in-depth distribution of the guest species. In spite of the limitations imposed by the validity of the used simplifying assumptions, the proposed methodology could complement existing methodologies for determining in-depth composition of hybrid organic-inorganic materials.

**Acknowledgements:** Financial support is gratefully acknowledged from the MEC Project CTQ2011-28079-CO3-02 which is supported with ERDF funds.

**References.**

- 1 D. R. Rolison and C. A. Bessel, *Acc. Chem. Res.*, 2000, **33**, 737–744.
- 2 A. Walcarius, in *Handbook of Zeolite Science and Technology*, ed. S. M. Auerbach, K. A. Carrado and P. K. Dutta, Marcel Dekker, New York, 2003, ch. 14.
- 3 A. Corma and H. García, *Top. Catal.*, 1998, **6**, 127–140.
- 4 J. C. Scaiano, H. García, *Acc. Chem. Res.*, 1999, **32**, 783–793.
- 5 H. Garcia and H. D. Roth, *Chem. Rev.*, 2002, **102**, 3947–4008.
- 6 K. Hoffmann and F. Marlon, in *Handbook of Zeolite Science and Technology*, ed. S. M. Auerbach, K.A. Carrado and P. K. Dutta, Marcel Dekker, New York, 2003, ch. 18.
- 7 G. Calzaferri, *Langmuir*, 2012, **28**, 6216–6231.
- 8 E. J. Anglin, L. Cheng, W. R. Freeman and M. J. Sailor, *Adv. Drug Deliv. Rev.*, 2008, **60**, 1266–1277.
- 9 B. P. Timko, K. Whitehead, W. Gao, D. S. Kohane, O. Farokhzad, D. Anderson and R. Langer, *Ann. Rev. Mater. Res.*, 2011, **41**, 1–20.
- 10 S. Bose and S. Tarafder, *Acta Biomaterialia*, 2012, **8**, 1401–1421.
- 11 S. Hashimoto, M. Hagiri, N. Matsubara and S. Tobita, *PhysChemChemPhys*, 2001, **3**, 5043–5051.
- 12 S. Hashimoto, M. Hagiri and S. Tobita, *PhysChemChemPhys*, 2002, **4**, 5856–5862.
- 13 S. Hashimoto, K. Uehara, K. Sogawa, M. Takada and H. Fukumura, *Phys.ChemChemPhys*, 2006, **8**, 1451–1458.
- 14 S. Hashimoto, *J. Phys. Chem. Lett.*, 2011, **2**, 509–519.
- 15 I. Gener, G. Bunitinx, A. Moissette and C. Bremard, *J. Phys. Chem. B*, 2002, **106**, 10322–10329.
- 16 E. H. Ellison, *J. Phys. Chem. B*, 2004, **108**, 4607–4618.
- 17 E. H. Ellison, *J. Phys. Chem. B*, 2005, **109**, 20424–20432.
- 18 E. H. Ellison, *J. Phys. Chem. B*, 2006, **110**, 11406–11414.
- 19 M. Alvaro, M. N. Chretien, V. Fornes, M. S. Galletero, H. Garcia and J.C. Scaiano, *J. Phys. Chem. B*, 2004, **108**, 16621–16625.

- 20 M. Alvaro, A. Corma, B. Ferrer, H. Garcia and E. Palomares, *PhysChemChemPhys*, 2004, **6**, 1345–1349.
- 21 P. Atienzar, A. Corma, H. Garcia and J. C. Scaiano, *Chem. Mater.*, 2004, **16**, 982–987.
- 22 S. Marquis, B. Ferrer, M. Alvaro, H. Garcia and H. D. Roth, *J. Phys. Chem. B*, 2006, **110**, 14956–14960.
- 23 S. Hashimoto, H. R. Moon and K. B. Yoon, *Micropor. Mesopor. Mater.*, 2007, **101**, 10–18.
- 24 Y. S. Lin, N. Yamamoto, Y. Choi, T. Yamaguchi, T. Okubo and S.I. Nakao, *Micropor. Mesopor. Mater.* 2000, **38**, 207–220.
- 25 D. F. Shantz and R. F. Lobo, *Chem. Mater.*, 1998, **10**, 4015–4024.
- 26 A. Barbon, M. Bellinazzi, M. Casagrande, L. Storaro, M. Lenarda and M. Brustolon, *PhysChemChemPhys*, 2006, **8**, 5069–5078.
- 27 M. Hureau, A. Moissette, S. Marquis, C. Brémard and H. Vezin, *PhysChemChemPhys*, 2009, **11**, 6299–6307.
- 28 B. Coasne, J. Haines, C. Levelut and G. Garbarino, *PhysChemChemPhys*, 2011, **13**, 20096–20099.
- 29 F. Scholz and B. Meyer, in *Electroanalytical Chemistry, A Series of Advances*, ed. A. J. Bard and I. Rubinstein, Marcel Dekker, New York, 1998, vol. 20, pp. 1–86.
- 30 F. Scholz, U. Schröder and R. Gulaboski, in *Electrochemistry of Immobilized Particles and Droplets*, Springer, Berlin-Heidelberg, 2005.
- 31 A. Doménech–Carbó, J. Labuda and F. Scholz, *Pure Appl. Chem.*, 2013, **85**, 609–631.
- 32 A. Doménech–Carbó, P. Formentín and H. García, *J. Phys. Chem. B*, 2002, **106**, 574–582.
- 33 A. Doménech–Carbó, H. García, M. Álvaro and E. Carbonell, *J. Phys. Chem. B*, 2003, **107**, 3040–3050.
- 34 A. Doménech–Carbó, M. T. Doménech–Carbó, M. L. Vázquez de Agredos–Pascual, *J. Phys. Chem. B*, 2006, **110**, 6027–6039.
- 35 A. Doménech–Carbó, M. T. Doménech–Carbó, M. Sánchez del Río, M. S. Goberna and E. Lima, *J. Phys. Chem. C*, 2009, **113**, 12118–12131.
- 36 A. Doménech–Carbó, in *Electrochemistry of Porous Materials*, Taylor&Francis, Boca Raton, 2010.

- 37 M. Lovric and F. Scholz, *J. Solid State Electrochem.*, 1997, **1**, 108–113.
- 38 M. Lovric, M. Hermes and F. Scholz, *J. Solid State Electrochem.*, 1998, **2**, 401–404.
- 39 K. B. Oldham, *J. Solid State Electrochem.*, 1998, **2**, 367–377.
- 40 M. Lovric and F. Scholz, *J. Solid State Electrochem.*, 1999, **3**, 172–175.
- 41 U. Schröder, K. B. Oldham, J. C. Myland, P. J. Mahon and F. Scholz, *J. Solid State Electrochem.*, 2000, **4**, 314–324.
- 42 A. Doménech–Carbó, M. T. Doménech–Carbó, M. Sánchez–Ramos and M. L. Vázquez de Agredos–Pascual, *J. Solid State Electrochem.* 2009, **13**, 869–878.
- 43 F. Scholz and M. Hermes, *Electrochem. Commun.* 1999, **1**, 345–348. (See corrigendum in *Electrochem. Commun.*, 2000, **2**, 814).
- 44 A. Doménech–Carbó, P. Formentín, H. García and M. J. Sabater, *Eur. J. Inorg. Chem.*, **2000**, 1339–1344.
- 45 A. Doménech–Carbó, S. Sánchez–Ramos, M. T. Doménech–Carbó, J. V. Gimeno–Adelantado, F. Bosch–Reig, D. J. Yusá–Marco and M. C. Saurí–Peris. *Electroanalysis*, 2002, **14**, 685–696.
- 46 A. Doménech–Carbó, M. Martini, L. Machado de Carvalho, M. T. Doménech–Carbó, *J. Electroanal. Chem.*, 2012, **684**, 13–19.
- 47 A. Doménech–Carbó, M. T. Doménech–Carbó, F. M. Valle–Algarra, M. E. Domine and L. Osete–Cortina, *J. Mater. Sci.* 2013, **48**, 7171–7183.
- 48 A. Doménech–Carbó, F. M. Valle–Algarra, M. T. Doménech–Carbó, M. E. Domine, L. Osete–Cortina, J. V. Gimeno–Adelantado, *Appl. Mater. Sci. Interfaces*, 2013, **5**, 8134–8145.
- 49 M. E. Haude, in *Identification and Classification of Colorants Used During Mexico's Early Colonial Period*, The American Institute for Conservation, 1997, vol. 60, pp. 1.
- 50 A. Wallert, *Mater. Res. Soc. Symp. Proc.* 1994, **352**, 653.
- 51 D. Magaloni, in *Pintural mural Prehispánica en México: área maya*, ed. B. de la Fuente and L. Satines–Cicero, Universidad Nacional Autónoma de México, México, 2001, pp. 85.
- 52 A. Doménech–Carbó, F. M. Valle–Algarra, M. T. Doménech–Carbó, M. E. Domine and L. Osete–Cortina, *RSC Advances*, 2013, **3**, 20099.
- 53 M. Arruebo, *Wiley Interdiscip. Rev. Nanomed. Manobiotech.* 2012, **4**, 16–30.

- 54 S. M. G. Pires, R. de Paula, M. M. Q. Simoes, A. M. S. Silva, M. R. M. Domingues, I. C. M. S. Santos, M. D. Vargas, V. F. Ferreira, M. G. P. M. S. Neves and J. A. S. Cavaleiro, *RSC Advances*, 2011, **1**, 1195–1199.
- 55 M. Niehues, V. P. Barros, F. da S. Emery, M. Dias-Baruffi, M. das D. Assis and N. P. Lopes, *Eur. J. Med. Chem.*, 2012, **54**, 804–812.
- 56 C.P. Andrieux, P. Hapiot, J.-M. Savéant, *J. Electroanal. Chem.* 1984, **117**, 49–65.
- 57 A. Doménech-Carbó, *J. Phys. Chem. B*, 2004, **108**, 20471–20478.
- 58 A. Doménech-Carbó, *J. Phys. Chem. C*, 2012, **116**, 25977–25983.
- 59 W. Oh and S. Nair, *Appl. Phys. Lett.*, 2005, **87**, 151912–151913.
- 60 J. M. Cases, Y. Grillet, M. François, L. Michot, F. Villieras, J. Yvon, *Clay Clay Miner.* 1991, **39**, 191–201.
- 61 E. Galan, *Clay Miner.* 1996, **31**, 442–453.
- 62 A.F. Drummond, C. Varajao, R.J. Gilkes, R.D. Hart, *Cáiz Clay Miner.* 2001, **49**, 44–55.
- 63 I.G. Casella, T.R.I. Cataldi, A.M. Salvi and E. Desimoni, *Anal. Chem.* 1993, **65**, 3143–3150.
- 64 P. A. L. Ferraz, F. C. de Abreu, A. V. Pinto, V. Glezer, J. Tonholo and M. O. F. Goulart, *J. Electroanal. Chem.*, 2001, **507**, 275–286.
- 65 F. C. Abreu, M. O. F. Goulart and A. M. Oliveira-Brett, *Electroanalysis*, 2002, **14**, 29–34.
- 66 E. Ngameni, I. K. Tonle, C. P. Nansu and R. Wandji, *Electroanalysis*, 2000, **12**, 847–852.
- 67 M. O. F. Goulart, N. M. F. Lima, A. E.-G. Sant’Ana, P. A. L. Ferraz, J. C. M. Cavalcanti, P. Falkowski, T. Ossowski and A. Liwo, *J. Electroanal. Chem.*, 2004, **566**, 25–29.
- 68 F. C. de Abreu, D. C. M. Ferreira, J. Wadhawan, C. Amatore, V. F. Ferreira, M. N. da Silva, M. C. B. V. de Souza, T. S. Gomes, E. A. Ximenes and M. O. F. Goulart, *Electrochem. Commun.*, 2005, **7**, 767–772.
- 69 H. R. Nasiri, M. Bolte and H. Schwalbe, *Nat. Prod. Res.*, 2008, **22**, 1225–1230.
- 70 A. Doménech-Carbó, M.T. Doménech-carbó, L. Osete-Cortina, N. Montoya, *Micropor. Mesopor. Mater.*, 2012, **166**, 123–130.
- 71 W. Turbeville, D. S. Robins and P. K. Dutta, *J. Phys. Chem.*, 1992, **96**, 5024–5029.
- 72 P. Lainé, M. Lanz and G. Calzaferri, *Inorg. Chem.*, 1996, **35**, 3514–3518.
- 73 D. Bruhwiler and G. Calzaferri, *Micropor. Mesopor. Mater.*, 2004, **72**, 1–23.

## Figures

**Figure 1.** Scheme for the advance of the diffusion layer through a solid film during solid-state voltammetric experiments at ion-permeable solids.

**Figure 2.** Variation of  $I (= i_p/v^{1/2})$  on  $v$  for CV at LA@PL<sub>25</sub>-modified electrodes immersed into 0.25 M HAc/NaAc aqueous solution at pH 4.75. Squares: peak C<sub>1</sub>; solid squares: peak A<sub>3</sub>.

**Figure 3.** a) SECM topographic image of a microparticulate deposit of LA@PL<sub>150</sub> on a glassy carbon plate in contact with aqueous acetate buffer using the Fe(CN)<sub>6</sub><sup>3-</sup>/Fe(CN)<sub>6</sub><sup>4-</sup> as a redox probe (see Experimental section). b) TEM image of a LA@PL<sub>150</sub> deposit prepared by equivalent drop casting method.

**Figure 4.** CV of microparticulate deposits of a,b) lapachol; c,d) LA@PL<sub>25</sub> specimens in contact with 0.25 M HAc/NaAc, pH 4.75. a,b) initial cathodic scan; c,d) initial anodic scan voltammograms. Potential scan rate 50 mV/s.

**Figure 5.** Voltammetry of graphite electrodes modified with a,b) LA@PL<sub>25</sub> and c,d) LA@PL<sub>150</sub> in contact with 0.25 M HAc/NaAc, pH 4.75. a,c) CV, potential scan rate 50 mV/s; b,d) SQWV, potential scan initiated at -0.75 V in the positive direction; potential step increment 4 mV; square wave amplitude 25 mV; frequency 5 Hz.

**Figure 6.** Structures of lapachol and related compounds and proposed electrochemical processes.

**Figure 7.** Chronoamperograms (two replicate curves) for a LA@PL<sub>150</sub> deposit on glassy carbon electrode (GCE) immersed into 0.25 M HAc/NaAc, pH 4.75. Applied potential -0.45 V.

**Figure 8.** Variation of  $c_j(x)/c_{\text{boundary}}$  calculated from CV data, using Eq. (18), for LA@PL<sub>25</sub> (solid squares), LA@PL<sub>150</sub> (squares), LA@KA<sub>25</sub> (solid triangles) and LA@KA<sub>150</sub> (triangles) taking  $D = 1.1 \times 10^{-11} \text{ cm}^2/\text{s}$ .

**Figure 9.** Variation of the  $i_p(A_3^{1st})/i_p(C_{1+2}^{2nd})$  ratio with the potential scan rate for CVs at PIGEs modified with LA@PL<sub>25</sub> (squares) and LA@PL<sub>150</sub> (solid squares) immersed into 0.25 M HAc/NaAc aqueous solution at pH 4.75.

**Figure 10.** In-depth variation of the  $\alpha_k^{ox}/\alpha_{boundary}^{ox}$  ratio in LA@PL<sub>25</sub> (solid squares) and LA@PL<sub>150</sub> (squares) specimens using CV data.

Figure 1.

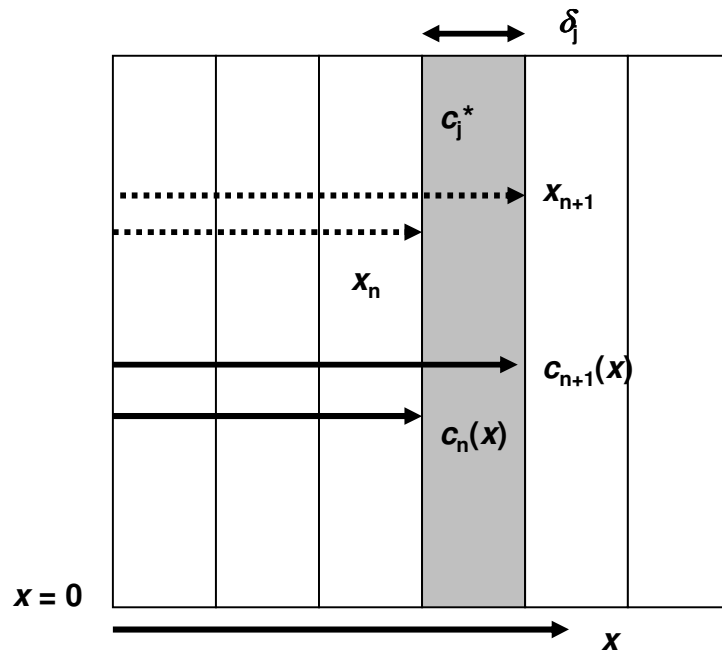


Figure 2.

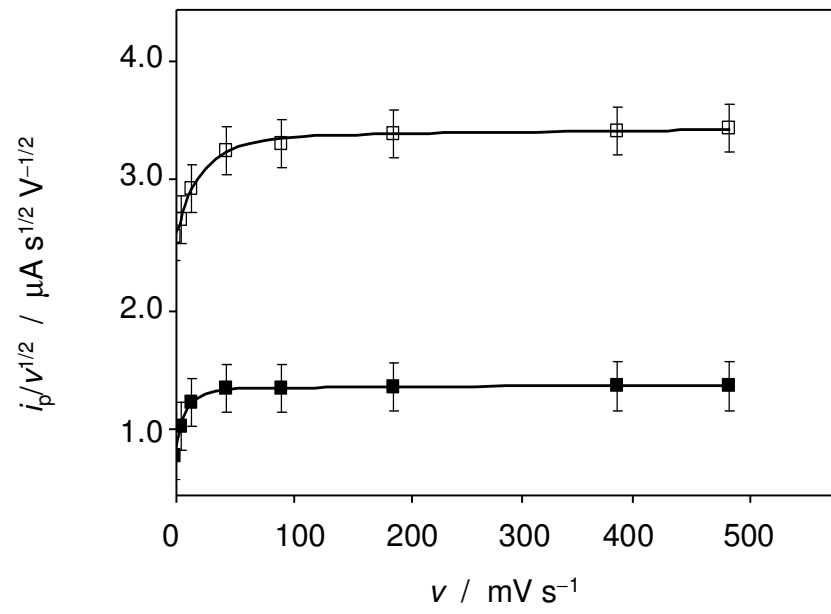


Figure 3.

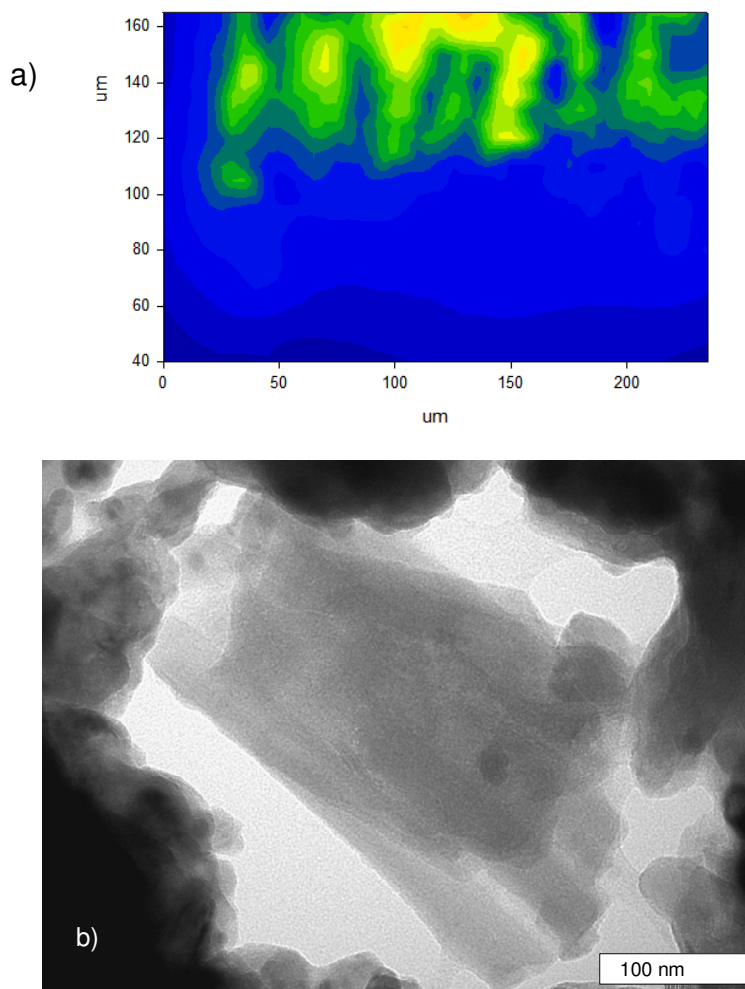


Figure 4.

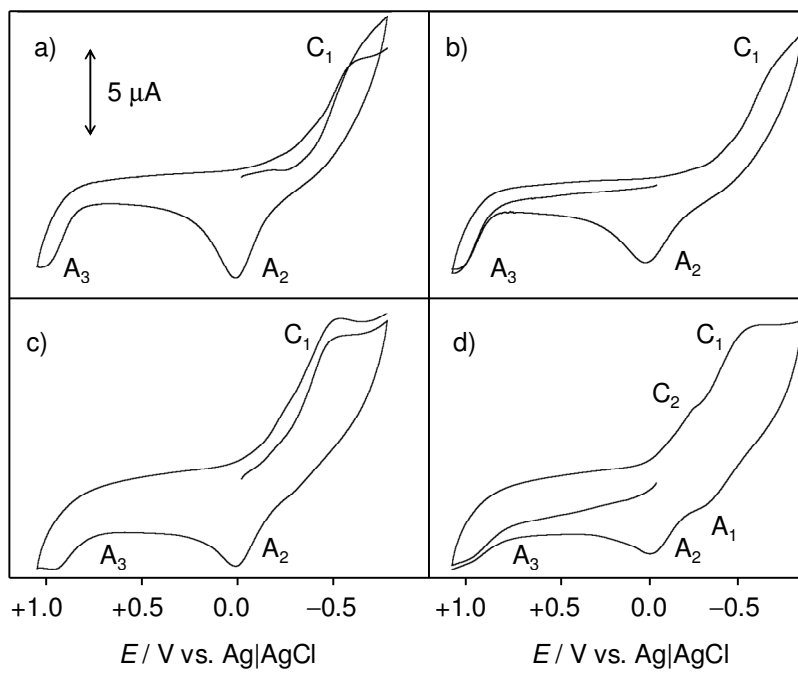


Figure 5.

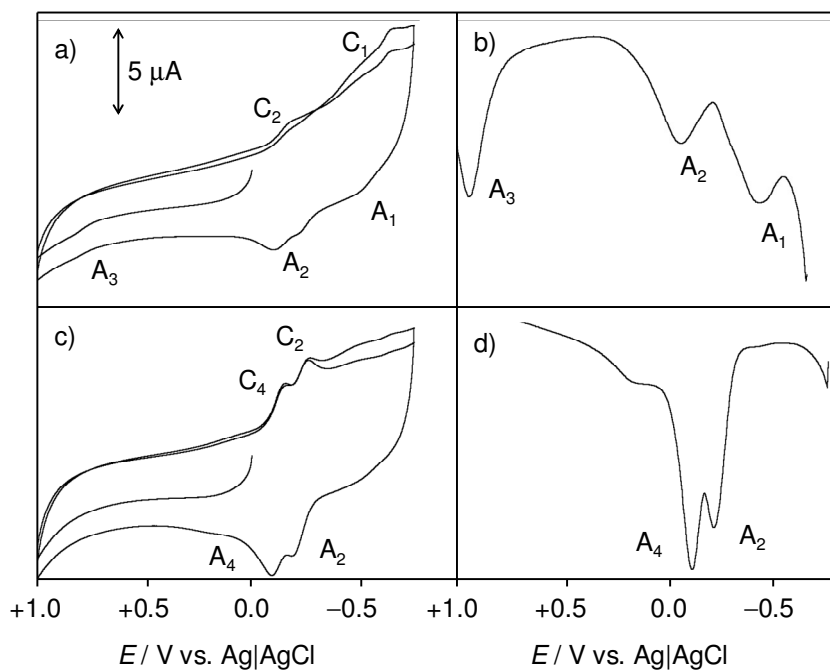


Figure 6.

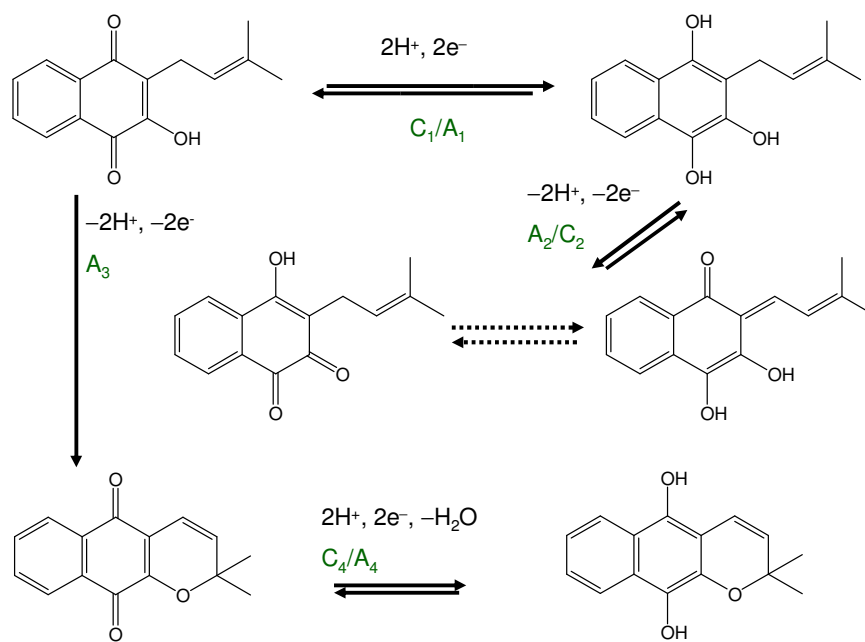


Figure 7.

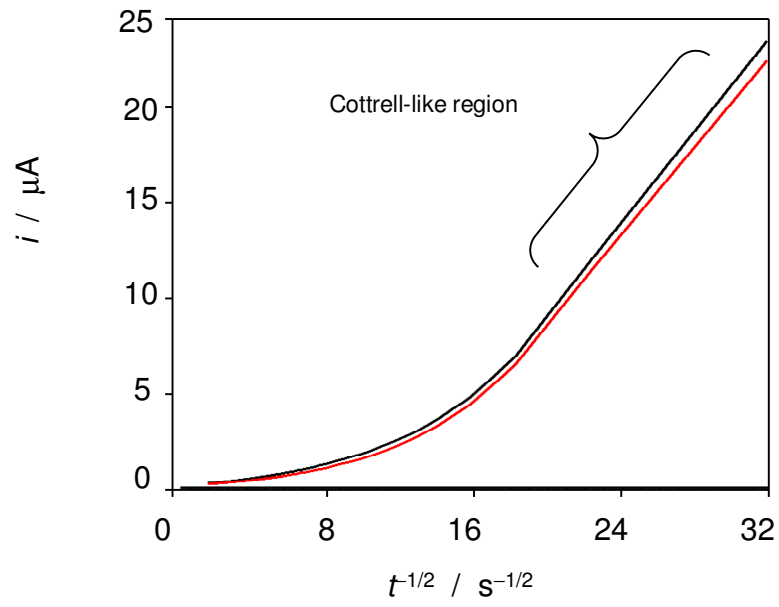


Figure 8.

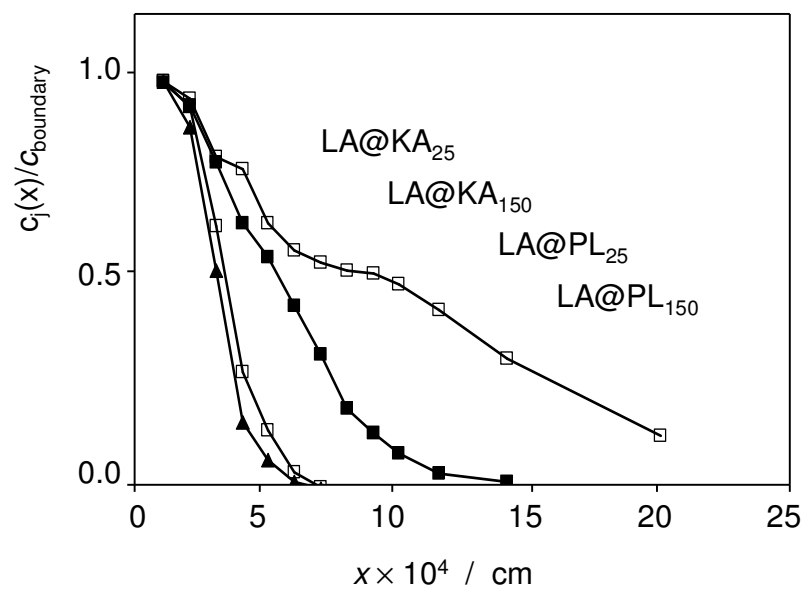


Figure 9.

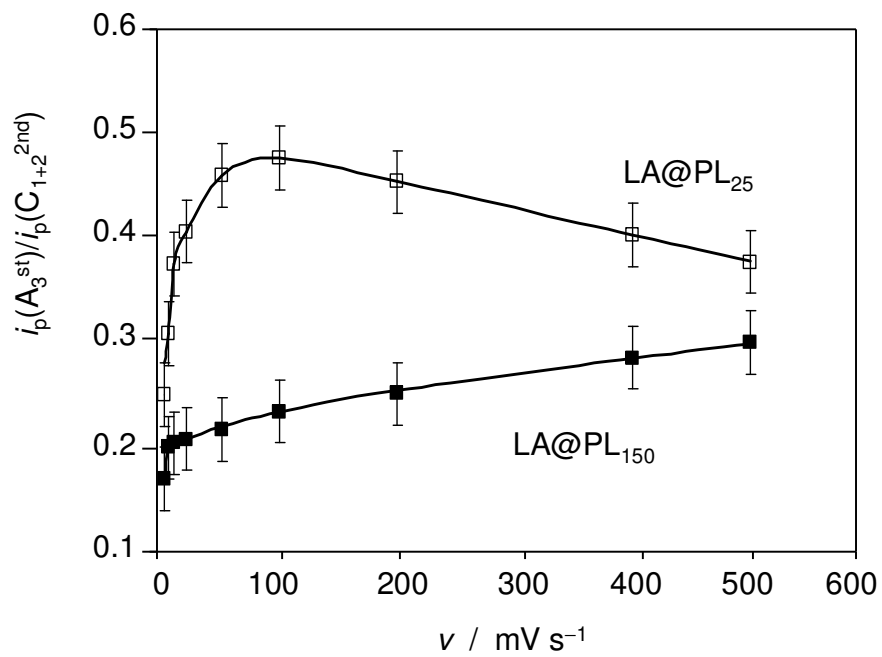


Figure 10.

